

The plasmoid instability during asymmetric inflow magnetic reconnection

Nicholas A. Murphy,^{1, a)} Aleida K. Young,^{1, 2} Chengcai Shen,^{1, 3, 4} Jun Lin,^{1, 3} and Lei Ni³

¹⁾Harvard-Smithsonian Center for Astrophysics, Cambridge, Massachusetts 02138, USA

²⁾Department of Atmospheric, Oceanic and Space Sciences, University of Michigan, Ann Arbor, Michigan 48109, USA

³⁾Yunnan Astronomical Observatory, Chinese Academy of Sciences, Kunming, Yunnan 650011, China

⁴⁾Graduate School of the Chinese Academy of Sciences, Beijing 100049, China

Theoretical studies of the plasmoid instability generally assume that the reconnecting magnetic fields are symmetric. We relax this assumption by performing two-dimensional resistive magnetohydrodynamic simulations of the plasmoid instability during asymmetric inflow magnetic reconnection. Magnetic asymmetry modifies the onset, scaling, and dynamics of this instability. Magnetic islands develop preferentially into the weak magnetic field upstream region. Outflow jets from individual X-points impact plasmoids obliquely rather than directly as in the symmetric case. Consequently, deposition of momentum by the outflow jets into the plasmoids is less efficient, the plasmoids develop net vorticity, and shear flow slows down secondary merging between islands. Secondary merging events have asymmetry along both the inflow and outflow directions. Downstream plasma is more turbulent in cases with magnetic asymmetry because islands are able to roll around each other after exiting the current sheet. As in the symmetric case, plasmoid formation facilitates faster reconnection for at least small and moderate magnetic asymmetries. However, when the upstream magnetic field strengths differ by a factor of four, the reconnection rate plateaus at a lower value than expected from scaling the symmetric results. We perform a parameter study to investigate the onset of the plasmoid instability as a function of magnetic asymmetry and domain size. There exist domain sizes for which symmetric simulations are stable but asymmetric simulations are unstable, suggesting that moderate magnetic asymmetry is somewhat destabilizing. We discuss the implications for plasmoid and flux rope formation in solar eruptions, laboratory reconnection experiments, and space plasmas. The differences between symmetric and asymmetric simulations provide some hints regarding the nature of the three-dimensional plasmoid instability.

I. INTRODUCTION

The Sweet-Parker model of magnetic reconnection¹ predicts the formation of very high aspect ratio current sheets in solar and astrophysical plasmas. However, these high Lundquist number current sheets are unstable to the formation of plasmoids.^{2–15} This plasmoid instability leads to significant departures from the classical view of laminar, Sweet-Parker-like reconnection.

Like the tearing mode,¹⁶ the linear properties of the plasmoid instability have been investigated analytically by performing an asymptotic matching analysis over an appropriate choice of equilibrium.^{2–6} The linear growth rate scales as $S^{1/4}V_A/L$ while the number of plasmoids scales as $S^{3/8}$. Here, V_A is the upstream Alfvén speed, L is the half-length of the current sheet, η is the resistivity, and $S \equiv LV_A/\eta$ is the Lundquist number. Numerical tests have confirmed these growth rates and determined the eigenmode structure.^{7, 8} That the growth rate scales as the Lundquist number to a positive exponent is significant: Sweet-Parker-like reconnection layers become more unstable with increasing Lundquist number. The positive exponent occurs in part because the thickness of Sweet-Parker current sheets scales as $\delta \sim S^{-1/2}$. In

contrast, the growth rate of the tearing instability scales as $S^{-3/5}$ for the constant- ψ regime and $S^{-1/3}$ for the nonconstant- ψ regime in slab geometry.¹⁷ In Hall MHD, the linear growth rate is enhanced when the ion inertial length exceeds the resistive skin depth.³ In three dimensions, oblique modes of the plasmoid instability may develop when a guide field is present because the locations of rational surfaces are not always the surface where the reconnecting component of the magnetic field reverses.⁴

Plasmoid formation has been shown to onset when the Lundquist number of a current sheet exceeds a critical value, S_c .^{6, 8, 10, 14, 18–20} The most commonly quoted value for the critical Lundquist number is $S_c \sim 10^4$, but there is considerable variation in the values found for S_c . Bhat-tacharjee *et al.*⁶ and Huang *et al.*⁸ find that S_c is around 3×10^4 or 4×10^4 , while Shen and coauthors¹⁴ determine that $S_c \approx 900$ for a different configuration. Ni *et al.*¹⁰ find that the onset criterion depends on the upstream plasma β , denoted β_0 . They find that S_c is between 2000 and 3000 for $\beta_0 = 0.2$, but this increases to between 8000 and 1×10^4 for $\beta_0 = 50$. They use isothermal initial conditions for most of their simulations, but find that many of the differences are reduced when uniform density initial conditions are used instead. The range in values for S_c indicates that the onset of the plasmoid instability is not just a function of the Lundquist number, but also depends on the configuration of the problem and the basic plasma parameters. The value (or range in values) for S_c

^{a)}Electronic mail: namurphy@cfa.harvard.edu

is important because statistical models of plasmoids^{20–23} often assume that individual plasmoids are separated by marginally stable current sheets.

The nonlinear evolution of the plasmoid instability has been investigated by several groups.^{6–15} Surprisingly, two-dimensional, symmetric resistive MHD simulations have shown that the dimensionless reconnection rate levels off at ~ 0.01 for $S \gtrsim S_c$.^{6,8} Reconnection is therefore fast (i.e., independent of the Lundquist number). Reconnection rates in solar flares typically range from ~ 0.001 to ~ 0.1 ,²⁴ and it has been argued that the role of the plasmoid instability is to trigger collisionless reconnection to allow reconnection rates closer to 0.1.^{9,12}

Most simulations of the plasmoid instability assume symmetric inflow. This approach reduces computing time because high resolution is required only near the symmetry axis and only half of the domain needs to be evolved in time. This simplifies the analysis because magnetic and velocity nulls located along the symmetry axis are easy to find. However, the reconnection process will in general have some asymmetry. Asymmetric inflow reconnection occurs when the upstream magnetic field strengths and/or densities differ.^{25–38} Such conditions occur at Earth’s dayside magnetopause^{39,40} and magnetotail,⁴¹ during turbulence,⁴² in laboratory plasma experiments,^{43–46} and in the solar atmosphere.^{47–50} Reconnection can also have asymmetric outflow,^{50–53} as well as three-dimensional asymmetries.⁵⁴

In this paper, we perform and analyze two-dimensional resistive MHD simulations of the plasmoid instability during asymmetric inflow magnetic reconnection. In Section II, we describe the numerical method and problem setup. In Section III, we present the simulation results and compare the nonlinear evolution of this instability during symmetric and asymmetric reconnection. In Section IV, we discuss how the onset criterion for this instability varies with asymmetry. Section V contains a discussion of the observational consequences of these simulations for the solar atmosphere, laboratory plasmas, and the magnetosphere. Section VI contains our discussion and conclusions.

II. NUMERICAL METHOD AND PROBLEM SETUP

The NIMROD code^{55,56} solves the equations of extended MHD using a finite element representation for two dimensions and a finite Fourier series expansion for the third dimension. In dimensionless form, the equations solved for the two-dimensional simulations reported in this paper are

$$\frac{\partial \rho}{\partial t} + \nabla \cdot (\rho \mathbf{V}) = \nabla \cdot D \nabla \rho, \quad (1)$$

$$\frac{\partial \mathbf{B}}{\partial t} = -\nabla \times (\eta \mathbf{J} - \mathbf{V} \times \mathbf{B}), \quad (2)$$

$$\mathbf{J} = \nabla \times \mathbf{B}, \quad (3)$$

$$\rho \left(\frac{\partial \mathbf{V}}{\partial t} + \mathbf{V} \cdot \nabla \mathbf{V} \right) = \mathbf{J} \times \mathbf{B} - \nabla p + \nabla \cdot \rho \nu \nabla \mathbf{V}, \quad (4)$$

$$\frac{\rho}{\gamma - 1} \left(\frac{\partial T}{\partial t} + \mathbf{V} \cdot \nabla T \right) = -\frac{p}{2} \nabla \cdot \mathbf{V} - \nabla \cdot \mathbf{q} + Q, \quad (5)$$

where the variables are given by: \mathbf{B} , magnetic field; \mathbf{V} , bulk plasma velocity; \mathbf{J} , current density; ρ , plasma density; p , plasma pressure; T , temperature; ν , kinematic viscosity; D , an artificial density diffusivity; and $\gamma = 5/3$, the ratio of specific heats. The heat source term includes Ohmic and viscous heating,

$$Q = \eta J^2 + \nu \rho \nabla \mathbf{V}^T : \nabla \mathbf{V}. \quad (6)$$

The heat flux vector is given by

$$\mathbf{q} = -\rho \left[\chi_{\parallel} \hat{\mathbf{b}} \hat{\mathbf{b}} + \chi_{\perp} (\mathbf{I} - \hat{\mathbf{b}} \hat{\mathbf{b}}) \right] \cdot \nabla T, \quad (7)$$

where $\hat{\mathbf{b}}$ is a unit vector in the direction of the magnetic field. The parallel and perpendicular thermal diffusivities are given by χ_{\parallel} and χ_{\perp} , respectively. The diffusivities are uniform and given by $\eta = 10^{-3}$, $\nu = 2 \times 10^{-3}$, $D = 10^{-3}$, $\chi_{\parallel} = 10^{-2}$, and $\chi_{\perp} = 5 \times 10^{-4}$. The normalizations are identical to those presented in Refs. 50 and 51. Divergence cleaning is used to prevent the accumulation of divergence error.⁵⁵

The initial conditions consist of a perturbed asymmetric Harris sheet with uniform density and no guide field.^{32,50} We define $\hat{\mathbf{x}}$ as the outflow direction, $\hat{\mathbf{y}}$ as the out-of-plane direction, and $\hat{\mathbf{z}}$ as the inflow direction. The initial equilibrium is given by

$$B_{x0}(z) = B_{R0} \left[\frac{\tanh\left(\frac{z}{\delta_0} - b\right) + b}{1 + b} \right], \quad (8)$$

$$p(z) = \frac{1}{2} (1 - B_x^2) + \beta_{R0} \frac{B_{R0}^2}{2}, \quad (9)$$

$$\rho(z) = 1 \quad (10)$$

Here, b controls the asymmetry of the magnetic field, δ_0 is the initial thickness of the current sheet, and $\beta_{R0} \equiv p_{R0} / (B_{R0}^2/2)$. Throughout this paper, the subscripts ‘L’ and ‘R’ correspond to the asymptotic initial amplitudes of fields for $z < 0$ and $z > 0$, respectively, while the subscript ‘0’ corresponds to $t = 0$. The ratio of the asymptotic upstream magnetic fields is given by

$$R \equiv \frac{B_L}{B_R}, \quad (11)$$

where we use the conventions that $B_L, B_R > 0$ and $B_L \leq B_R$ such that $0 < R \leq 1$. Because R is a function of time, we compare simulations using R_0 instead. We take $B_{R0} = 1$ and $\beta_{R0} = 1$ for all simulations. Because B_{R0} is kept constant and B_{L0} is decreased for asymmetric cases, it is important to note that there is consequently less magnetic flux and energy available during asymmetric simulations. To maintain total pressure balance, plasma

pressure is higher on the weak magnetic field side such that $p_{L0} > p_{R0}$ and $\beta_{L0} > \beta_{R0}$ when $R_0 < 1$.

Each simulation is seeded with initial magnetic perturbations of the form

$$\mathbf{B}_p(x, z) = \sum_{q=1}^{N_q} \nabla \times (A_q \hat{\mathbf{y}}), \quad (12)$$

where

$$A_q = -B_q \Delta \exp \left[- \left(\frac{x - x_q}{\Delta} \right)^2 - \left(\frac{z}{\Delta} \right)^2 \right]. \quad (13)$$

Multiple perturbations are used so that the initial conditions are not symmetric about $x = 0$. The simulations presented in Section III have stronger secondary initial perturbations than the simulations in Section IV.

The domain consists of m_x by m_z rectangular finite elements along the outflow and inflow directions, respectively. Sixth order finite elements are used for all simulations. The size of the computational domain is given by $x \in [-x_{\max}, x_{\max}]$ and $z \in [-z_{\max}, z_{\max}]$, where x_{\max} varies between simulations and $z_{\max} = 16$ for all simulations. We model four different initial asymmetries: $R_0 \in \{0.125, 0.25, 0.5, 1.0\}$ (with $R_0 = 0.125$ only considered in Section IV). For our largest simulations with $x_{\max} = 150$, we use $(m_x, m_z) = (576, 32)$ for $R_0 = 1$, $(m_x, m_z) = (336, 60)$ for $R_0 = 0.5$, and $(m_x, m_z) = (306, 60)$ for $R_0 = 0.25$. We use no-slip, conducting wall boundaries for each upstream region. The simulations are periodic along the outflow direction; consequently, downstream pressure effects are likely to be more important than in simulations with open outflow boundary conditions.

During simulations with $R_0 = 1$, significant mesh packing is required over a relatively small portion of the computational domain. During simulations with $R_0 \neq 1$, most X-points slowly drift into the strong field upstream region.^{27,50} Consequently, high resolution along the inflow direction is required over a larger portion of the domain. Relatively high resolution is required along the outflow direction for all plasmoid unstable simulations so that secondary reconnection associated with island merging can be sufficiently resolved. Insufficient resolution often yields spurious nulls as a result of numerical dispersion error (see also Ref. 57). The resolution requirements along the outflow direction are most stringent for cases with $R_0 = 1$. Higher resolution is required in the weak field upstream region than in the strong field upstream region. When initializing these simulations, we chose to increase resolution in the current sheet region to ensure convergence rather than increasing z_{\max} ; consequently, the late-time evolution of asymmetric simulations is impacted somewhat by the conducting wall boundary on the weak magnetic field side.

During the initial simulations performed for this study, we used relatively large amplitude symmetric initial perturbations with a characteristic length scale compar-

able to the size of the computational domain. Simulations starting from these initial conditions showed plasma sloshing back and forth along the inflow direction, suggesting that there was a large-scale pressure imbalance in our initial conditions. As an analogy, consider two regions of antiparallel magnetic field that are initially in total pressure equilibrium but have different magnetic field amplitudes, B_0 and $R_0 B_0$ with $0 < R_0 < 1$. Then suppose that the magnetic field strength in each region is decreased by δB . The weak magnetic field region will then have a total pressure that is $(1 - R_0) B_0 \delta B$ greater than the strong magnetic field side, resulting in a large-scale force imbalance. We greatly reduced the sloshing behavior by using localized, small amplitude initial perturbations.

For symmetric simulations, it is straightforward to find magnetic and velocity nulls located on the symmetry axis, $z = 0$. To determine the null positions, we find neighboring grid points between which the signs of B_z or V_x change and apply Brent's method.⁵⁸ Brent's method combines the robustness of bisection and root bracketing for ill-behaved functions while using inverse quadratic interpolation which converges quickly for well-behaved functions. The finite element basis functions are used to interpolate between grid points. Magnetic nulls are classified as X-type if $\frac{\partial B_z}{\partial x} \frac{\partial B_x}{\partial z} > 0$ and O-type if $\frac{\partial B_z}{\partial x} \frac{\partial B_x}{\partial z} < 0$.

For asymmetric simulations and to find nulls not located along the symmetry axis during symmetric simulations, we combine several techniques to find magnetic and velocity nulls. First, we search for grid cells with changes in sign for both components of the vector field while excluding cells along the conducting wall boundaries. Second, we use bilinear interpolation⁵⁹ to provide an initial approximation for the null position. We exclude cases where the inferred location is outside the grid cell boundary. Rarely, this step finds multiple nulls within the same grid cell. While bilinear or trilinear interpolation is highly appropriate for simulations with fields defined only at discrete locations, higher order accuracy can be obtained for NIMROD simulations by interpolating the finite element basis functions. Our third step is to perform a few iterations of the method of steepest descent on the magnitude of the vector field. This method is robust but converges slowly. Fourth, we use Broyden's method⁶⁰ to converge on the null position. If Broyden's method does not converge, we alternate between the third and fourth steps until convergence is achieved. To classify magnetic nulls, we define a matrix \mathbf{M} with elements $M_{ij} = \partial B_i / \partial x_j$. The null is X-type if $\det \mathbf{M} < 0$ and O-type if $\det \mathbf{M} > 0$.⁶¹

Finally, we define several quantities to facilitate our analysis and comparisons between different simulations. When investigating the scaling of asymmetric inflow reconnection, Refs. 27 and 62 derived that the outflow velocity scales as a hybrid Alfvén speed that is a function of the magnetic field strengths and densities in both up-

stream regions,

$$V_{Ah} \equiv \sqrt{\frac{B_L B_R (B_L + B_R)}{\rho_L B_R + \rho_R B_L}}. \quad (14)$$

This simplifies to $V_{Ah0} = \sqrt{R_0}$ when $B_{R0} = 1$ and $\rho_0 = \rho_{L0} = \rho_{R0} = 1$. This corresponds to $V_{Ah0} = 1$ for $R_0 = 1$, $V_{Ah0} \approx 0.71$ for $R_0 = 0.5$, $V_{Ah0} = 0.5$ for $R_0 = 0.25$, and $V_{Ah0} \approx 0.35$ for $R_0 = 0.125$. Throughout this paper, we use the convention

$$L \equiv \frac{2}{3} x_{\max}. \quad (15)$$

to account for the current sheet not extending the entire distance along the outflow direction. Using these quantities, we define the hybrid Lundquist number to be⁵⁰

$$S_h \equiv \frac{LV_{Ah}}{\eta}. \quad (16)$$

The reconnection rate for collisional asymmetric reconnection without plasmoids is predicted to be²⁷

$$E_{\text{predict}} = \sqrt{\frac{\eta V_{Ah}}{L} B_L B_R}. \quad (17)$$

Using our conventions that $\rho_{L0} = \rho_{R0} = 1$, $R_0 = B_{L0}/B_{R0}$, and $B_{R0} = 1$, we find that

$$E_{\text{predict},0} = R_0^{3/4} \eta^{1/2} L^{-1/2}. \quad (18)$$

This expression is an exact result for our conventions and our use of dimensionless parameters, but should not be considered a general result.

To describe the dynamics of X-points and O-points, we define $\mathbf{x}_n = (x_n, z_n)$ as the position of a magnetic null. The plasma flow velocity at the null is $\mathbf{V}(\mathbf{x}_n)$. The time derivative of the null's position is $d\mathbf{x}_n/dt$. In resistive MHD, differences between $\mathbf{V}(\mathbf{x}_n)$ and $d\mathbf{x}_n/dt$ must be due to resistive diffusion of the magnetic field. In general, $\mathbf{V}(\mathbf{x}) \neq d\mathbf{x}_n/dt$ when asymmetry is present and $\eta > 0$. For O-points, we have generally found that $\mathbf{V}(\mathbf{x}_n) \approx d\mathbf{x}_n/dt$. For X-points, the difference can be a non-negligible fraction of the nearby Alfvén speed.^{50,51} During X-line retreat in resistive MHD, Ref. 51 has shown that the physical mechanism behind this difference is resistive diffusion of the inflow component of the magnetic field along the inflow direction.

III. SIMULATION RESULTS

In this section, we compare simulations of the plasmoid instability during symmetric inflow reconnection and asymmetric inflow reconnection.

A. Nonlinear Dynamics

During the plasmoid instability with symmetric inflow (Fig. 1), the X-points and O-points within the current sheet region are located along $z = 0$ because of symmetry. Some X-points and O-points develop away from $z = 0$ in the downstream region away from the current sheet. Within the current sheet, the outflow jets impact each island directly so that momentum from the jets is transported efficiently into the islands. The islands do not develop net vorticity [Fig. 1(g)]. The quadrupole structure in V_z around large islands corresponds to upstream plasma being temporarily pushed out of the way as the island moves along with the reconnection outflow; this also corresponds to reverse flow in V_x in the upstream region as plasma flows back to fill the area behind the moving island. The flow patterns in the outflow region show some degree of order because of the assumption of symmetry, and thus are not best described as being turbulent [Figs. 1(e) and 1(f); cf. Ref. 15]. There exist several flow stagnation points (in the simulation reference frame) along $z = 0$ as well as symmetrically in both upstream regions. Often, flow stagnation points along the symmetry axis are located between an X-point and a more central maximum in plasma pressure. This occurs because flow stagnation points preferentially occur where pressure gradient and tension forces cancel.^{51,52} Individual X-points are often located in proximity to a neighboring magnetic island so that the small-scale reconnection has asymmetric outflow. The plasma flow velocity at each individual X-point differs somewhat from the velocity of each X-point [$\mathbf{V}(\mathbf{x}_n) \neq d\mathbf{x}_n/dt$] such that there is net plasma flow across each X-point.⁵¹

There exist many qualitative differences between the symmetric and asymmetric plasmoid instability (Fig. 2). In contrast to the symmetric case, the positions along the inflow direction of the X-points and O-points in the current sheet are not constrained to $z = 0$. The X-points generally drift slowly into the strong field upstream region.^{27,50} In general, the X-points closer to $x = 0$ are displaced more into the strong field upstream region than X-points in the periphery. When islands merge with each other or the large island downstream of the reconnection region, X-points sometimes end up being displaced into the weak field upstream region. Because of field line rigidity, very little happens in the strong field upstream region.

The most apparent feature of the plasmoid instability during asymmetric inflow reconnection is that the plasmoids develop preferentially into the weak field upstream region [Fig. 2(a)]. The effect has been noted in prior simulations of asymmetric inflow reconnection without secondary island formation.^{26,27,33,50} Reconnection outflow jets therefore impact islands obliquely rather than directly. This has two main consequences for the structure and dynamics of individual plasmoids. First, the islands develop net vorticity as seen in Fig. 2(g). This effect has been observed in prior simulations of line-tied

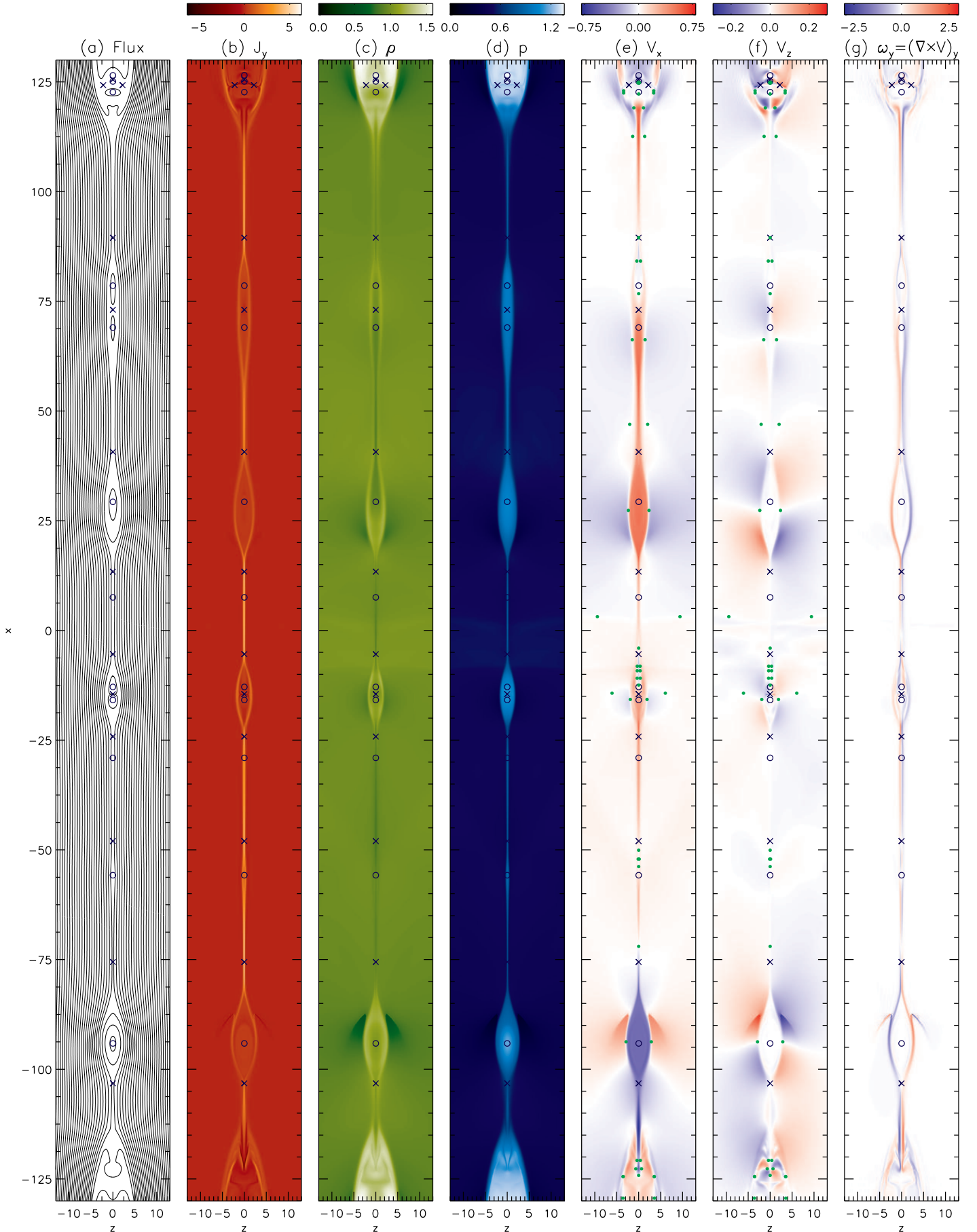


FIG. 1. Simulation of the plasmoid instability with symmetric inflow ($R_0 = 1$) at $t = 324$. Shown are contours of the (a) magnetic flux; (b) out-of-plane current density, J_y ; (c) plasma density, ρ ; (d) plasma pressure, p ; (e) the outflow component of velocity, V_x ; (f) the inflow component of velocity, V_z ; and (g) the vorticity, $\omega_y = (\nabla \times \mathbf{V})_y$. X-points are denoted by ‘x’ and O-points are denoted by ‘o’. The green dots in panels (e) and (f) represent flow stagnation points.

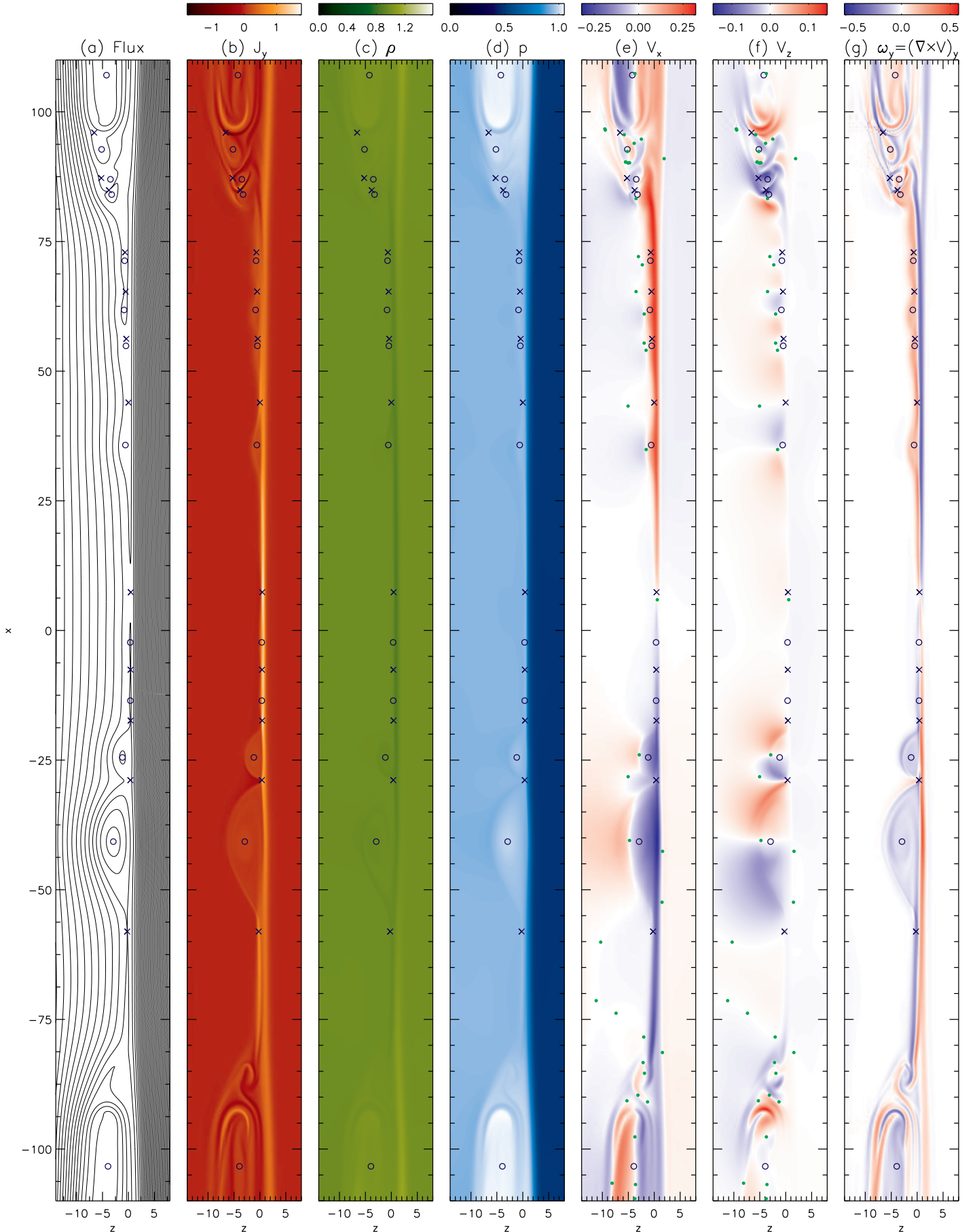


FIG. 2. Simulation of the plasmoid instability with asymmetric inflow ($R_0 = 0.25$) at $t = 731$. Shown are contours of the (a) magnetic flux; (b) out-of-plane current density, J_y ; (c) plasma density, ρ ; (d) plasma pressure, p ; (e) the outflow component of velocity, V_x ; (f) the inflow component of velocity, V_z ; and (g) the vorticity, ω_y . X-points are denoted by 'x' and O-points are denoted by 'o'. The green dots in panels (e) and (f) represent flow stagnation points.

asymmetric reconnection.⁵⁰ Second, momentum transport from the reconnection outflow jets into the islands is less efficient. The reconnection outflow is able to partially bypass the islands. Consequently, the islands that form during asymmetric inflow reconnection have slower velocities relative to V_{Ah0} . For the largest cases with $x_{\max} = 150$, islands propagate at velocities of $\lesssim 0.5V_{A0}$ for $R_0 = 1$ and at velocities of $\lesssim 0.3V_{Ah0}$ for $R_0 = 0.25$. Islands that develop in asymmetric simulations therefore remain in the current sheet for significantly longer.

Secondary merging events occur during both symmetric and asymmetric simulations when two islands reconnect with each other to form a single island. The flux contained in the resulting island equals the greater of the two initial fluxes.²³ An example of secondary merging during a symmetric simulation is the X-point at $x = -14.5$ between two neighboring magnetic islands in Figure 1 (see also the X-point at $x = 73.1$ for an earlier stage of secondary merging). During symmetric simulations, the outflow from secondary reconnection events is symmetric, but the inflow is generally asymmetric because merging islands typically have different sizes. The secondary outflow jets are impeded symmetrically by the upstream magnetic field. Prior scaling studies show that symmetric obstructions reduce the reconnection rate much more effectively than when only one outflow jet is obstructed.⁵² However, because there is no freedom for plasmoids to roll around each other, secondary reconnection is able to be more effective.

During simulations with $R_0 \neq 1$, the reconnection process has asymmetry along both the inflow and outflow directions. An instance of secondary merging late in the simulation with $x_{\max} = 150$ and $R_0 = 0.25$ is shown in Fig. 3. The characteristic magnetic field strength is 0.1 in the island, which corresponds to a local upstream Alfvén speed of 0.1 given that $\rho \approx 1$. At this time, $\mathbf{x}_n = (-38.40, -1.62)$, $\mathbf{V}(\mathbf{x}_n) = (-0.100, -0.018)$, and $d\mathbf{x}_n/dt = (-0.098, -0.040)$; this indicates that the net plasma flow across the X-point along the z direction is ~ 0.22 of the local upstream Alfvén speed. The tilting of the current sheet occurs because the island below is larger than the island above.

The most important feature of this secondary reconnection is the flow pattern shown in Fig. 3(a) in the reference frame of the moving X-point. The characteristic inflow/outflow pattern typically associated with two-dimensional resistive reconnection is absent. In contrast, the flow pattern in the current sheet region is dominated by shear flow associated with the vorticity in the islands. The magnitude of the shear flow is comparable to the local upstream Alfvén speed (rather than the hybrid Alfvén speed), which has been shown to suppress and slow down the reconnection process.⁶³ The merging process began around $t \approx 765$ [when the X-point between these two islands first had $J_y(\mathbf{x}_n) < 0$] and was not quite complete by the end of the simulation at $t = 1021$. This velocity shear does not occur during secondary merging in symmetric simulations because those islands lack net vorticity.

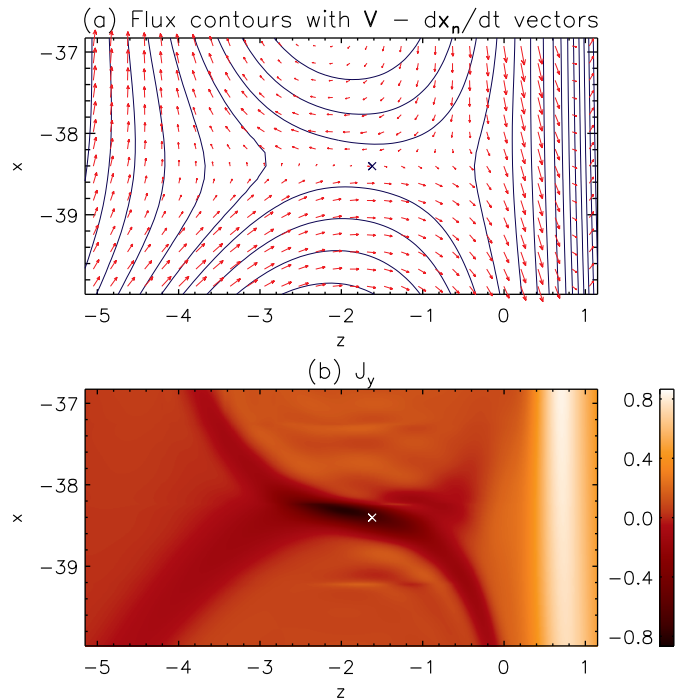


FIG. 3. Secondary merging between two plasmoids at $t = 818$ for $R_0 = 0.25$ and $x_{\max} = 150$. Shown are (a) magnetic flux contours and velocity vectors in the frame of the moving X-point, $\mathbf{V} - d\mathbf{x}_n/dt$, and (b) out-of-plane current density, J_y . The local flow pattern is dominated by shear flow associated with island vorticity. The longest vector corresponds to a velocity of 0.17 while the characteristic Alfvén speed in the islands is ~ 0.1 . The X-point is denoted by ‘x’.

B. Reconnection Rate

A key result from two-dimensional resistive MHD simulations of the symmetric plasmoid instability is that the reconnection rate becomes insensitive to the Lundquist number for $S > S_c$. We now investigate how the reconnection rate is impacted by magnetic asymmetry during the plasmoid instability.

We define the reconnection rate, $E_{y,\max}$, to be the maximum out-of-plane electric field among all X-points within the current sheet, $-L \leq x \leq L$. This directly represents the amount of flux being reconnected at the most active X-point. An alternative method used for symmetric simulations is to compare the inflow velocity to the outflow velocity; however, this results in some ambiguity for asymmetric inflow simulations because X-points drift at different velocities along the inflow direction, and the inflow velocities differ in each upstream region.

Fig. 4 shows the reconnection rate over time for simulations with different magnetic asymmetries, $R_0 \in \{0.25, 0.5, 1.0\}$, and different domain sizes, $x_{\max} \in \{9.375, 18.75, 37.5, 75, 150\}$. Plasmoids develop for all simulations with $x_{\max} \geq 37.5$, but do not develop or are not important for simulations with $x_{\max} \leq 18.75$. At

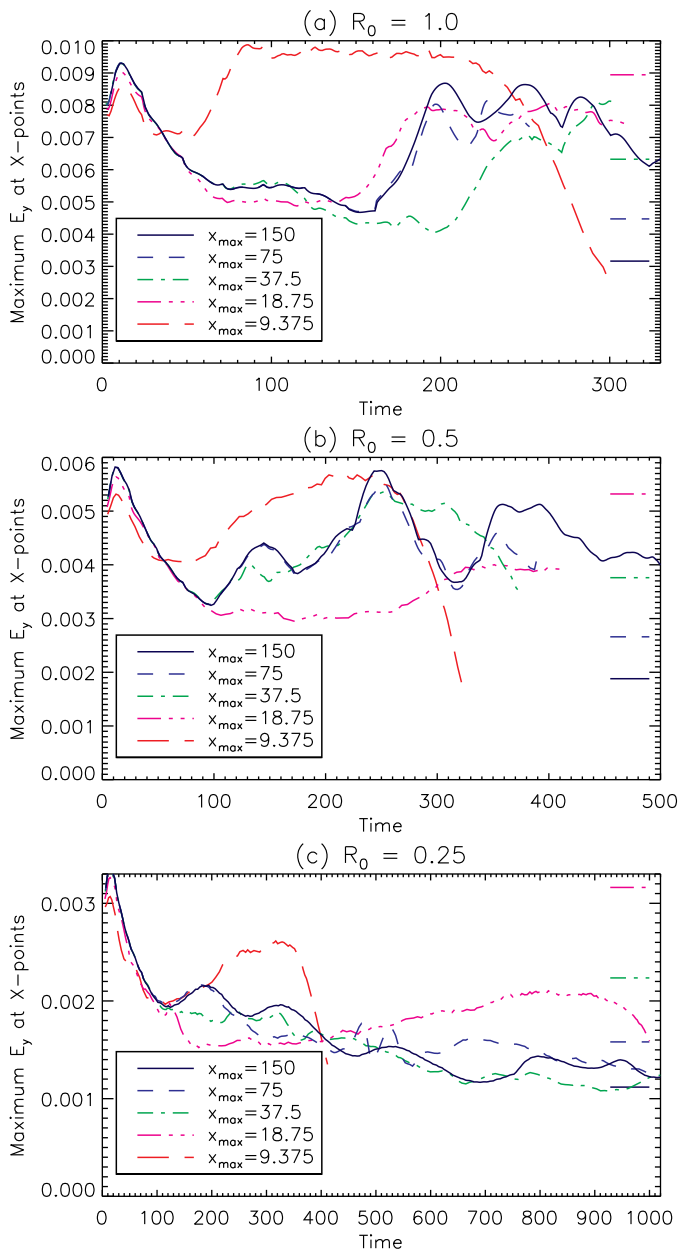


FIG. 4. The reconnection rate as a function of time for simulations with different asymmetries and domain sizes. The reconnection rate is given by the maximum out-of-plane electric field among all of the X-points in a simulation. The horizontal line segments indicate the reconnection rate predicted by Eq. 18. The predictions for $x_{\max} = 9.375$ are not shown, but are factors of $\sqrt{2}$ greater than the predictions for $x_{\max} = 18.75$.

$t = 0$, $E_{y,\max}$ is large because the initial current sheet is thin, so we concentrate our analysis on $t \gtrsim 75/V_{Ah0}$ after reconnection develops.

We use two strategies to compare the reconnection rates between different simulations. The first strategy is to compare small and large simulations directly, without considering predicted values for the reconnection rate. Nominally, the effects not included in theoretical models

such as viscosity, thermal conduction, and downstream pressure will have similar consequences in each simulation. The second strategy is to compare $E_{y,\max}$ with the predicted value given by Eq. 18. This method allows us to determine the extent to which additional factors are responsible for slowing down the reconnection rate.

In symmetric simulations [Fig. 4(a)], the peak reconnection rate is only weakly sensitive to changes in the domain size (and therefore Lundquist number). The peak reconnection rate for $x_{\max} = 9.375$ is comparable to the peak reconnection rate for $x_{\max} = 150$. For cases without plasmoids, Eq. 18 overpredicts the reconnection rate. This indicates that effects not included in the derivation of this equation slow down reconnection. Overall, this result corroborates the reconnection rate enhancement due to the plasmoid instability found in previous works.^{6,8,14,20} The reconnection rate levels off at $E_{y,\max} \sim 0.008$.

For $R_0 = 0.5$ [Fig. 4(b)], the results are qualitatively similar to $R_0 = 1$. The peak reconnection rates are comparable among most simulations. The exception is $x_{\max} = 18.75$ which has a slower reconnection rate than the rest of the simulations. The plasmoid instability continues to show enhancement of the reconnection rate for this asymmetry. The reconnection rate levels off between about 0.004 and 0.005, which is consistent with what one would expect from the symmetric results and the scaling for our simulation setup that $E_{y,\max} \propto R_0^{3/4}$.

There are some qualitative differences for $R_0 = 0.25$ [Fig. 4(c)]. The peak reconnection rates for the cases without plasmoids are higher than the cases with plasmoids. However, the reconnection rates for the three cases with plasmoids are comparable, indicating that the reconnection rate is leveling off as the domain size is increased. Therefore, we conclude that there remains enhancement of the reconnection rate due to the plasmoid instability. However, when we compare to the predicted values from Eq. 18, the reconnection rates from the simulation are generally much lower. For the largest two domain sizes, the prediction becomes comparable to the simulation results. The reconnection rate levels off at $E_{y,\max}$ between about 0.0012 and 0.0015, compared to the value of 0.0028 expected from scaling the symmetric case.

Overall, we conclude that the reconnection rate is still enhanced due to the plasmoid instability at least for asymmetries of $0.25 \lesssim R_0 \leq 1$. However, for $R_0 = 0.25$, the reconnection rate levels off at a lower value than would be inferred from the symmetric results. For low to moderate asymmetries, the enhancement in the reconnection rate is comparable to what would be expected from scaling the symmetric case.

IV. ONSET OF INSTABILITY

In this section, we perform a grid of nonlinear simulations with different domain sizes and magnetic asym-

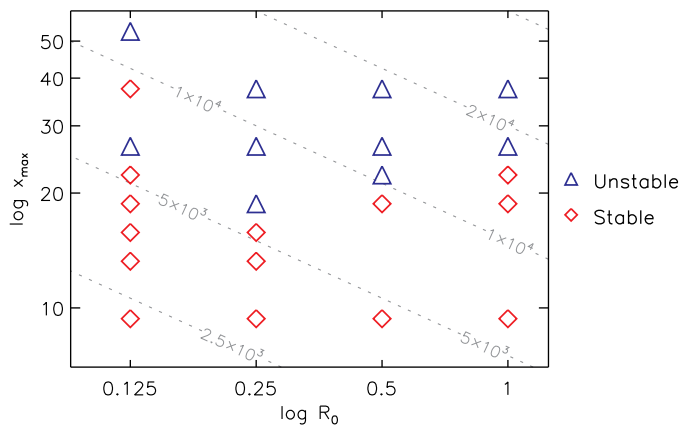


FIG. 5. Results from a parameter study to test the dependence of the initial magnetic asymmetry ratio, $R_0 \in \{0.125, 0.25, 0.50, 1.00\}$, and the half-size of the computational domain along the outflow direction, x_{\max} , on the onset of the plasmoid instability. Simulations are classified as unstable if new X-points form in the current sheet before $t = 5x_{\max}/V_{Ah0}$. Blue triangles indicate instability, while red diamonds indicate stability. The gray dotted lines are contours of constant initial hybrid Lundquist number, S_{h0} .

metries to investigate the onset criterion of the plasmoid instability during symmetric and asymmetric inflow magnetic reconnection. We vary the initial magnetic asymmetry, R_0 , and the size of the computational domain along the outflow direction, x_{\max} . We place a single perturbation at the origin, and a much smaller perturbation off to one side to allow outflow asymmetry. Simulations are classified as unstable if new X-points appear in the current sheet region before $t = 5x_{\max}/V_{Ah0}$. If no new X-points form, then the simulations are classified as stable. For a given asymmetry, the smallest unstable simulation typically yields only short-lived islands that exit the current sheet and merge with the main outflow island soon after formation. The results of this parameter study are shown in Fig. 5.

For symmetric cases, we find the critical Lundquist number to be $S_c \approx 1.6 \times 10^4$. This is somewhat smaller than the Huang *et al.*⁸ value of $S_c \sim 4 \times 10^4$, comparable to Loureiro *et al.*²⁰ value of $S_c \sim 1.2 \times 10^4$, and larger than the values reported by Ni *et al.*¹⁰ and Shen *et al.*¹⁴ The differences between these values occur in part because the onset criterion depends on the configuration and plasma parameters as well as the Lundquist number.

For asymmetric cases, we initially hypothesized that plasmoids form when the hybrid Lundquist number exceeds a critical value, S_{ch} , which is a constant and not a function of asymmetry. This hypothesis predicts system sizes for which the symmetric case is unstable and asymmetric cases are stable, and that the demarcation between stable and unstable configurations are aligned with a contour of constant S_{h0} . However, Fig. 5 indicates that this hypothesis is incorrect.

Figure 5 shows that plasmoids form for smaller do-

main sizes when there is a moderate magnetic asymmetry, $R_0 \in \{0.25, 0.5\}$, than when there is symmetry, $R_0 = 1$. For $R_0 = 1.0, 0.5, 0.25$, and 0.125 , the smallest unstable domain sizes are $x_{\max} = 26.52, 22.30, 18.75$, and 26.52 , respectively. In contrast to our hypothesis, moderate magnetic asymmetry is somewhat destabilizing for the plasmoid instability.

Anomalously, the simulation with $R_0 = 0.125$ and $x_{\max} = 37.5$ does not show plasmoid formation out to $t = 7x_{\max}/V_{Ah0}$ despite new X-lines forming in a smaller simulation with $x_{\max} = 26.52$. New X-lines do appear for $x_{\max} = 53.03$. When the simulations with $R_0 = 0.125$ were repeated with different initial perturbations, none of them showed evidence for plasmoid formation for $x_{\max} \leq 37.5$. These results suggest that strong magnetic asymmetry ($R_0 \lesssim 0.125$) is stabilizing.

We now consider possibilities for why moderate magnetic asymmetry cases show plasmoid formation for shorter domain sizes than symmetric cases. Our first hypothesis was that there was simply inadequate time for plasmoids in the symmetric case to form. To test this, we ran the largest stable symmetric simulation (with $R_0 = 1$ and $x_{\max} = 22.30$) twice as long. No new X-points developed in the extended run of this simulation, so this hypothesis is not supported. Our second hypothesis was that the difference in the flow properties led to the difference in the onset domain size. This could be caused by either the outflow being slower such that there is more time for instabilities to develop, or that there will be less shear flow stabilization for cases with slower outflow. We test this hypothesis by repeating the largest stable and smallest unstable simulations for different asymmetries with $Pm = 0.5$ and $Pm = 8$ instead of $Pm = 2$ (where $Pm = \nu/\eta$ is the magnetic Prandtl number). In contrast to the prediction of this hypothesis, higher viscosity leads to larger domain sizes becoming stable. This hypothesis is not supported; however, an important caveat is that changing the viscosity affects the structure of the diffusion region as well as slowing down the outflow. The results do not rule out an alternative hypothesis that the development of the instability is correlated with intermittency in the flow.

The results from this parameter study do not explain why simulations with moderate asymmetry are unstable for smaller domain sizes than symmetric cases, or why strongly asymmetric simulations are more stable. Some insight may be gained by performing a linear stability analysis for the plasmoid instability during asymmetric inflow reconnection, including an asymptotic matching analysis and linear simulations,^{2,5,16,64} to see how the growth rate and eigenmode structure are modified by magnetic asymmetry.

V. OBSERVATIONAL CONSEQUENCES

In this section, we make observational predictions for the behavior of plasmoids in solar, laboratory, and space

plasmas during asymmetric inflow reconnection. Differences between simulation and observation will provide key insights into the roles of important effects not included in the simulations, such as collisionless effects and three-dimensional effects.

A. Solar Atmosphere

The standard model of solar eruptions predicts the formation of an elongated current sheet in the wake behind the rising flux rope.⁶⁵ While unambiguous identification of these structures is difficult without magnetic field information, several features classified as current sheets have been observed in the solar corona.^{66,67} These current sheets necessarily have asymmetric outflow and may have asymmetric inflow.^{49,50} Large blobs are frequently observed during these events⁶⁶ which have been interpreted to be the result of a tearing or plasmoid instability.⁶⁸ ‘Monster plasmoids’ such as those predicted by Ref. 21 are the most likely features to be observed.

In principle, an offset of blobs toward the weak field upstream region could be seen with instruments such as the Atmospheric Imaging Assembly (AIA) on the Solar Dynamics Observatory, the X-Ray Telescope on Hinode, and the Large Angle and Spectrometric Coronagraph (LASCO) on the Solar and Heliospheric Observatory. However, if the current sheet is observed at a small angle with respect to the line of sight, then blobs that are physically offset might not show an apparent offset due to projection effects. Constraints on the overall geometry are therefore vital. High-resolution, high-cadence observations by AIA have been used to investigate vorticity in current sheet features at low heights,⁶⁹ and it may be possible to find evidence for vorticity in current sheet blobs. However, the time cadence of LASCO observations is too slow to observe vorticity on the scales of individual blobs.

Asymmetric reconnection also occurs during solar jets,⁴⁸ which happen when newly emerged flux reconnects with pre-existing, overlying flux.⁷⁰ The pre-existing flux is usually weaker, so our simulations predict plasmoid development preferentially into that region as well as the associated vortical motions. However, the spatial and temporal resolution requirements to observe small-scale structure and vortical motions during jet reconnection are likely beyond the capabilities of current instrumentation.

B. Laboratory Experiments

The current generation of dedicated laboratory experiments on magnetic reconnection are stable or marginally stable against the formation of multiple plasmoids or flux ropes.⁷¹ There is hope that the next generation of reconnection experiments will have $S > S_c$ to allow the plasmoid instability to be investigated in the laboratory. If

the geometry is toroidal or cylindrical, then the reconnection process will necessarily have asymmetric inflow unless the radius is very large. In the Magnetic Reconnection Experiment (MRX), reconnection is driven by ramping up or down currents carried within toroidal flux cores. During the ‘pull’ mode of operation (see Fig. 5 of Ref. 43), the low radius side of the current sheet has stronger magnetic field than the high radius upstream region, and the current sheet gradually drifts toward lower radii.^{44,72,73}

It is therefore likely that the effects discussed in this paper will play some role in the dynamics of the plasmoid instability in future experiments. The asymmetry is not expected to be large, so the effects are not likely to be as pronounced as in the simulations. For future experiments with configurations similar to MRX but with $S > S_c$, our simulations predict the development of flux ropes preferentially into the high radius upstream region and the development of net vorticity. The current sheet is expected to drift toward lower radii where the magnetic field is stronger. Secondary reconnection is expected to be less efficient than predicted by two-dimensional, symmetric simulations because of the freedom of flux ropes to roll around each other, especially in the downstream region. However, these predictions are likely to be modified due to cylindrical geometry effects not included in our paper. Simulations of the plasmoid instability in an experimental geometry will allow direct comparisons to be made (see also Refs. 44, 73–75).

C. Space Plasmas

Plasmoids and flux ropes are frequently observed *in situ* during reconnection events in planetary magnetospheres and the solar wind. Reconnection events at the dayside magnetopause and its flanks have asymmetric inflow.^{39,76} In contrast to our two-dimensional resistive MHD simulations with an antiparallel magnetic field configuration, reconnection in near-Earth space plasmas is in the collisionless regime.^{41,77,78} There is often a guide field, and shear flow effects are often important for dayside reconnection.²⁵ There is also density asymmetry along with magnetic asymmetry.

For these reasons, we anticipate that there will be significant qualitative differences between our simulations and *in situ* observations of asymmetric reconnection at the dayside magnetopause. Nevertheless, some of the macroscopic features of our simulations may remain applicable during collisionless asymmetric inflow reconnection. Island development into the weak field upstream region is in principle observable; pragmatically, this will be difficult to diagnose because of the limited number of spacecraft taking measurements. More promising are measurements of vorticity in secondary flux ropes formed by reconnection (see Ref. 76 and references therein), but care will be needed to distinguish these features from Kelvin-Helmholtz vortices. To allow more direct com-

parisons to *in situ* observations, it will be important to extend recently performed two-fluid,^{28,29} hybrid,³⁷ and fully kinetic^{30,33,34,36–38} simulations of asymmetric inflow reconnection to investigate the dynamics of secondary islands and flux ropes.

VI. DISCUSSION

In this paper, we perform resistive MHD simulations of the plasmoid instability during magnetic reconnection with asymmetric upstream magnetic fields. This is in contrast to most studies of the plasmoid instability which assume that the reconnection process is symmetric. Relaxing the assumption of symmetric inflow leads to qualitatively different results.

During symmetric simulations, the X-points and O-points within the current sheet region are located along the symmetry axis so that momentum from the outflow jets is efficiently transported into the islands. Secondary islands within the current sheet do not develop net vorticity and are advected quickly out of the current sheet. Secondary reconnection events associated with island merging have symmetric outflow but asymmetric inflow. In the downstream region, some X-points and O-points are located away from the symmetry axis. Because of the assumption of symmetry, the flow pattern in the downstream region is structured and therefore not best described as being turbulent.

During asymmetric simulations, the locations of the X-points and O-points are offset from each other along the inflow direction. There is generally slow drifting of the current sheet into the strong field upstream region. X-points near the center of the sheet are displaced further into the strong field upstream region than X-points near the current sheet exits. Not much happens in the strong field upstream region because of field line rigidity. Islands develop preferentially into the weak field upstream region. Consequently, outflow jets impact the islands obliquely rather than directly so that net vorticity develops and momentum transport into the islands is less efficient. During secondary reconnection, shear flow associated with vorticity in the merging islands slows down reconnection. The downstream regions develop a complicated flow structure indicative of turbulence, with islands able to roll around each other as well as merge.

We compare the reconnection rate enhancement between symmetric and asymmetric cases. During high Lundquist number symmetric simulations, the reconnection rate is enhanced above the value predicted from the Sweet-Parker model. This is consistent with previous work.^{6,8,14,20} During simulations with a magnetic asymmetry of $R_0 = 0.5$, the reconnection rate enhancement is comparable to what is expected from scaling the symmetric simulations. For stronger asymmetry ($R_0 = 0.25$), the reconnection rate is still enhanced by the presence of plasmoids in the current sheet, but to less of a degree than for $R_0 \in \{0.5, 1.0\}$. Scaling from the symmetric

simulations to $R_0 = 0.25$ cases overpredicts the reconnection rate.

We perform an onset study of the plasmoid instability for both symmetric and asymmetric inflow reconnection. For the symmetric case, we find that the critical Lundquist number for the onset of the instability is $S_c \approx 1.6 \times 10^4$. This is consistent with the canonical result that onset occurs when the Lundquist number is of order 10^4 . Interestingly, we find that there exist domain sizes for which the symmetric case is stable but moderate asymmetry cases (e.g., $R_0 \in \{0.25, 0.5\}$) are unstable. This suggests that moderate asymmetry has a destabilizing influence on the formation of plasmoids. However, our results indicate that strong asymmetry (e.g., $R_0 \lesssim 0.125$) has a stabilizing influence.

We predict observational consequences for the asymmetric plasmoid instability in the solar atmosphere, laboratory experiments, and space plasmas. The most likely characteristics to be observed are the development of islands preferentially into the weak field upstream region and vorticity in the plasmoids. In the solar atmosphere, high spatial and temporal resolution will be required and projection effects will make interpretation difficult. Future laboratory experiments may naturally have asymmetric inflow due to cylindrical geometry effects, although the asymmetry may be relatively modest. *In situ* observations of flux ropes formed during asymmetric inflow reconnection at Earth's dayside magnetopause provide an opportunity to test predictions based on vorticity of secondary islands; however, collisionless effects not included in our simulations are expected to be important. For all of these situations, discrepancies between simulations and observations will provide insight into the roles of three-dimensional and collisionless effects.

Our simulations of the plasmoid instability during asymmetric inflow reconnection hint at the nature of this instability in three dimensions. In particular, outflow jets from individual, small-scale reconnection sites are more likely to impact flux ropes obliquely rather than directly. This may cause momentum transport from the jets into the flux ropes to be less efficient and vorticity in the flux ropes to develop. Vorticity in flux ropes may lead to shear flow stabilization when flux ropes merge. Consequently, secondary merging of flux ropes formed by the plasmoid instability should not necessarily be assumed to be efficient (see also Ref. 79). As in the downstream region of our asymmetric simulations, flux ropes will likely have additional freedom to roll around each other while merging or instead of merging. However, further study of the three-dimensional plasmoid instability will be required before solid conclusions can be drawn.

There remain several open questions and promising areas of future work regarding the plasmoid instability during both symmetric and asymmetric inflow magnetic reconnection. Thus far, no analytical theory exists that describes the linear properties of the plasmoid instability during asymmetric inflow reconnection; however, the effects of asymmetry on the tearing mode have been

investigated.⁶⁴ The role of collisionless effects and the transition to collisionless reconnection have been investigated for the symmetric plasmoid instability^{9,12} but not for the asymmetric case. The role of three-dimensional effects during the plasmoid instability requires further study. Additional investigation of the role of a guide field will provide more insight into real situations, especially for three-dimensional and fully kinetic simulations. Statistical models of magnetic islands in current sheets^{20–23} will need to be extended in order to incorporate asymmetry and three-dimensional effects.

ACKNOWLEDGMENTS

The authors thank A. Bhattacharjee, P. A. Cassak, T. G. Forbes, L. Guo, Y.-M. Huang, K. E. Korreck, N. F. Loureiro, M. Oka, J. C. Raymond, K. K. Reeves, S. L. Savage, L. S. Shepherd, C. R. Sovinec, and H. D. Winter for useful discussions. The authors thank members of the NIMROD team for ongoing code development that helped make this work possible. In particular, we thank J. King for suggesting memory management strategies that allowed larger simulations to be performed. Resources supporting this work were provided by the NASA High-End Computing (HEC) Program through the NASA Advanced Supercomputing (NAS) Division at Ames Research Center. This research has benefited greatly from the use of NASA’s Astrophysics Data Service.

This research was supported by NASA grants NNX09AB17G, NNX11AB61G, and NNX12AB25G; NASA contract NNM07AB07C; and NSF SHINE grant AGS-1156076 to the Smithsonian Astrophysical Observatory. A.K.Y. acknowledges support from the NSF-REU solar physics program at the Center for Astrophysics, grant number ATM-0851866.

- ¹P. A. Sweet, in *Electromagnetic Phenomena in Cosmical Physics*, IAU Symposium, Vol. 6, edited by B. Lehnert (1958) p. 123; E. N. Parker, *J. Geophys. Res.* **62**, 509 (1957); *Astrophys. J. Supp.* **8**, 177 (1963).
- ²N. F. Loureiro, A. A. Schekochihin, and S. C. Cowley, *Phys. Plasmas* **14**, 100703 (2007).
- ³S. D. Baalrud, A. Bhattacharjee, Y.-M. Huang, and K. Germaschewski, *Phys. Plasmas* **18**, 092108 (2011).
- ⁴S. D. Baalrud, A. Bhattacharjee, and Y.-M. Huang, *Phys. Plasmas* **19**, 022101 (2012).
- ⁵L. Ni, K. Germaschewski, Y.-M. Huang, B. P. Sullivan, H. Yang, and A. Bhattacharjee, *Phys. Plasmas* **17**, 052109 (2010).
- ⁶A. Bhattacharjee, Y.-M. Huang, H. Yang, and B. Rogers, *Phys. Plasmas* **16**, 112102 (2009).
- ⁷R. Samtaney, N. F. Loureiro, D. A. Uzdensky, A. A. Schekochihin, and S. C. Cowley, *Phys. Rev. Lett.* **103**, 105004 (2009).
- ⁸Y.-M. Huang and A. Bhattacharjee, *Phys. Plasmas* **17**, 062104 (2010).
- ⁹Y.-M. Huang, A. Bhattacharjee, and B. P. Sullivan, *Phys. Plasmas* **18**, 072109 (2011).
- ¹⁰L. Ni, U. Ziegler, Y.-M. Huang, J. Lin, and Z. Mei, *Phys. Plasmas* **19**, 072902 (2012).
- ¹¹L. Ni, I. I. Roussev, J. Lin, and U. Ziegler, *Astrophys. J.* **758**, 20 (2012).

- ¹²L. S. Shepherd and P. A. Cassak, *Phys. Rev. Lett.* **105**, 015004 (2010).
- ¹³M. Bárta, J. Büchner, M. Karlický, and J. Skála, *Astrophys. J.* **737**, 24 (2011).
- ¹⁴C. Shen, J. Lin, and N. A. Murphy, *Astrophys. J.* **737**, 14 (2011).
- ¹⁵Z. Mei, C. Shen, N. Wu, J. Lin, N. A. Murphy, and I. I. Roussev, *Mon. Not. R. Astron. Soc.* **425**, 2824 (2012).
- ¹⁶H. P. Furth, J. Killeen, and M. N. Rosenbluth, *Phys. Fluids* **6**, 459 (1963).
- ¹⁷B. Coppi, R. Galvão, R. Pellat, M. Rosenbluth, and P. Rutherford, *Sov. J. Plasma Phys.* **2**, 533 (1976).
- ¹⁸D. Biskamp, *Phys. Fluids* **29**, 1520 (1986).
- ¹⁹H. Baty, *Phys. Plasmas* **19**, 092110 (2012).
- ²⁰N. F. Loureiro, R. Samtaney, A. A. Schekochihin, and D. A. Uzdensky, *Phys. Plasmas* **19**, 042303 (2012).
- ²¹D. A. Uzdensky, N. F. Loureiro, and A. A. Schekochihin, *Phys. Rev. Lett.* **105**, 235002 (2010).
- ²²Y.-M. Huang and A. Bhattacharjee, *Phys. Rev. Lett.* **109**, 265002 (2012).
- ²³R. L. Fermo, J. F. Drake, and M. Swisdak, *Phys. Plasmas* **17**, 010702 (2010).
- ²⁴K. P. Dere, *Astrophys. J.* **472**, 864 (1996); J. Qiu, J. Lee, D. E. Gary, and H. Wang, *Astrophys. J.* **565**, 1335 (2002); H. Isobe, H. Takasaki, and K. Shibata, *Astrophys. J.* **632**, 1184 (2005); J. Jing, J. Qiu, J. Lin, M. Qu, Y. Xu, and H. Wang, *Astrophys. J.* **620**, 1085 (2005); K. Nagashima and T. Yokoyama, *Astrophys. J.* **647**, 654 (2006); N. Narukage and K. Shibata, *Astrophys. J.* **637**, 1122 (2006).
- ²⁵A. L. La Belle-Hamer, A. Otto, and L. C. Lee, *J. Geophys. Res.* **100**, 11875 (1995).
- ²⁶M. Ugai, *Phys. Plasmas* **7**, 867 (2000).
- ²⁷P. A. Cassak and M. A. Shay, *Phys. Plasmas* **14**, 102114 (2007).
- ²⁸P. A. Cassak and M. A. Shay, *Geophys. Res. Lett.* **35**, 19102 (2008).
- ²⁹P. A. Cassak and M. A. Shay, *Phys. Plasmas* **16**, 055704 (2009).
- ³⁰K. Malakit, M. A. Shay, P. A. Cassak, and C. Bard, *J. Geophys. Res.* **115**, A10223 (2010).
- ³¹J. E. Borovsky and M. Hesse, *Phys. Plasmas* **14**, 102309 (2007).
- ³²J. Birn, J. E. Borovsky, and M. Hesse, *Phys. Plasmas* **15**, 032101 (2008); J. Birn, J. E. Borovsky, M. Hesse, and K. Schindler, *Phys. Plasmas* **17**, 052108 (2010).
- ³³P. L. Pritchett, *J. Geophys. Res.* **113**, 6210 (2008).
- ³⁴P. L. Pritchett and F. S. Mozer, *J. Geophys. Res.* **114**, 11210 (2009).
- ³⁵K. G. Tanaka, A. Retinò, Y. Asano, M. Fujimoto, I. Shinohara, A. Vaivads, M. Khotyaintsev, Y. André, M. B. Bavassano-Cattaneo, S. C. Buchert, and C. J. Owen, *Ann. Geophys.* **26**, 2471 (2008).
- ³⁶K. G. Tanaka, M. Fujimoto, and I. Shinohara, *Int. J. Geophys.* **2010**, 202583 (2010).
- ³⁷N. Aunai, M. Hesse, S. Zenitani, M. Kuznetsova, C. Black, R. Evans, and R. Smets, *Phys. Plasmas* **20**, 022902 (2013).
- ³⁸M. Swisdak, B. N. Rogers, J. F. Drake, and M. A. Shay, *J. Geophys. Res.* **108**, 1218 (2003).
- ³⁹T. D. Phan and G. Paschmann, *J. Geophys. Res.* **101**, 7801 (1996); H. C. Ku and D. G. Sibeck, *J. Geophys. Res.* **102**, 2243 (1997); G. Paschmann, M. Øieroset, and T. Phan, *Space Sci. Rev.* **1** (2013).
- ⁴⁰H. Hasegawa, J. Wang, M. W. Dunlop, Z. Y. Pu, Q.-H. Zhang, B. Lavraud, M. G. G. T. Taylor, O. D. Constantinescu, J. Berchem, V. Angelopoulos, J. P. McFadden, H. U. Frey, E. V. Panov, M. Volwerk, and Y. V. Bogdanova, *Geophys. Res. Lett.* **37**, 16101 (2010).
- ⁴¹M. Øieroset, T. D. Phan, and M. Fujimoto, *Geophys. Res. Lett.* **31**, 12801 (2004).
- ⁴²S. Servidio, W. H. Matthaeus, M. A. Shay, P. A. Cassak, and P. Dmitruk, *Phys. Rev. Lett.* **102**, 115003 (2009); S. Servidio, W. H. Matthaeus, M. A. Shay, P. Dmitruk, P. A. Cassak, and M. Wan, *Phys. Plasmas* **17**, 032315 (2010).
- ⁴³M. Yamada, H. Ji, S. Hsu, T. Carter, R. Kulsrud, N. Bretz,

- F. Jobs, Y. Ono, and F. Perkins, *Phys. Plasmas* **4**, 1936 (1997).
- ⁴⁴N. A. Murphy and C. R. Sovinec, *Phys. Plasmas* **15**, 042313 (2008).
- ⁴⁵M. T. Beidler and P. A. Cassak, *Phys. Rev. Lett.* **107**, 255002 (2011).
- ⁴⁶B. Rogers and L. Zakharov, *Phys. Plasmas* **2**, 3420 (1995).
- ⁴⁷M. G. Linton, *J. Geophys. Res.* **111**, 12 (2006).
- ⁴⁸N. Nakamura, K. Shibata, and H. Isobe, *Astrophys. J.* **761**, 87 (2012).
- ⁴⁹Y. Su and A. van Ballegooijen, *Astrophys. J.* **764**, 91 (2013).
- ⁵⁰N. A. Murphy, M. P. Miralles, C. L. Pope, J. C. Raymond, H. D. Winter, K. K. Reeves, D. B. Seaton, A. A. van Ballegooijen, and J. Lin, *Astrophys. J.* **751**, 56 (2012).
- ⁵¹N. A. Murphy, *Phys. Plasmas* **17**, 112310 (2010).
- ⁵²N. A. Murphy, C. R. Sovinec, and P. A. Cassak, *J. Geophys. Res.* **115**, 9206 (2010).
- ⁵³M. Oka, M. Fujimoto, T. K. M. Nakamura, I. Shinohara, and K.-I. Nishikawa, *Phys. Rev. Lett.* **101**, 205004 (2008); K. K. Reeves, J. A. Linker, Z. Mikić, and T. G. Forbes, *Astrophys. J.* **721**, 1547 (2010); K. Galsgaard and I. Roussev, *Astron. Astrophys.* **383**, 685 (2002).
- ⁵⁴N. Katz, J. Egedal, W. Fox, A. Le, J. Bonde, and A. Vrublevskis, *Phys. Rev. Lett.* **104**, 255004 (2010); J. Egedal, N. Katz, J. Bonde, W. Fox, A. Le, M. Porkolab, and A. Vrublevskis, *Phys. Plasmas* **18**, 111203 (2011); A. K. Al-Hachami and D. I. Pontin, *Astron. Astrophys.* **512**, A84 (2010); D. I. Pontin, *Adv. Space Res.* **47**, 1508 (2011); V. S. Lukin and M. G. Linton, *NPGEO* **18**, 871 (2011); S. Dorfman, H. Ji, M. Yamada, J. Yoo, E. Lawrence, C. Myers, and T. D. Tharp, *Geophys. Res. Lett.* **40**, 233 (2013); P. F. Wyper and R. Jain, *Phys. Plasmas* **20**, 052901 (2013).
- ⁵⁵C. R. Sovinec, A. H. Glasser, T. A. Gianakon, D. C. Barnes, R. A. Nebel, S. E. Kruger, D. D. Schnack, S. J. Plimpton, A. Tarditi, and M. S. Chu, *J. Comput. Phys.* **195**, 355 (2004).
- ⁵⁶C. R. Sovinec, J. R. King, and the NIMROD Team, *J. Comput. Phys.* **229**, 5803 (2010).
- ⁵⁷M. Wan, W. H. Matthaeus, S. Servidio, and S. Oughton, *Phys. Plasmas* **20**, 042307 (2013).
- ⁵⁸R. P. Brent, *Algorithms for Minimization Without Derivatives* (Englewood Cliffs, NJ: Prentice Hall, 1973) Chap. 3-4.
- ⁵⁹A. L. Haynes and C. E. Parnell, *Phys. Plasmas* **14**, 082107 (2007).
- ⁶⁰C. G. Broyden, *Mathematics of Computation* **19**, 577 (1965).
- ⁶¹C. E. Parnell, J. M. Smith, T. Neukirch, and E. R. Priest, *Phys. Plasmas* **3**, 759 (1996).
- ⁶²M. Swisdak and J. F. Drake, *Geophys. Res. Lett.* **34**, L11106 (2007).
- ⁶³X. L. Chen and P. J. Morrison, *Phys. Fluids B* **2**, 495 (1990); Q. Chen, A. Otto, and L. C. Lee, *J. Geophys. Res.* **102**, 151 (1997); R. J. La Haye, D. P. Brennan, R. J. Buttery, and S. P. Gerhardt, *Phys. Plasmas* **17**, 056110 (2010); J. H. Li and Z. W. Ma, *J. Geophys. Res.* **115**, A09216 (2010); P. A. Cassak, *Phys. Plasmas* **18**, 072106 (2011); P. A. Cassak and A. Otto, *Phys. Plasmas* **18**, 074501 (2011).
- ⁶⁴M. Dubois and A. Samain, *Plasma Physics* **21**, 101 (1979); G. Einaudi and F. Rubini, *Nuovo Cimento B Serie* **81**, 102 (1984); D. Q. Ding, L. C. Lee, and C. F. Kennel, *J. Geophys. Res.* **97**, 8257 (1992).
- ⁶⁵J. Lin and T. G. Forbes, *J. Geophys. Res.* **105**, 2375 (2000).
- ⁶⁶Y.-K. Ko, J. C. Raymond, J. Lin, G. Lawrence, J. Li, and A. Fludra, *Astrophys. J.* **594**, 1068 (2003); S. Takasao, A. Asai, H. Isobe, and K. Shibata, *Astrophys. J.* **745**, L6 (2012).
- ⁶⁷A. Ciaravella, J. C. Raymond, J. Li, P. Reiser, L. D. Gardner, Y.-K. Ko, and S. Fineschi, *Astrophys. J.* **575**, 1116 (2002); D. F. Webb, J. Burkepile, T. G. Forbes, and P. Riley, *J. Geophys. Res.* **108**, 1440 (2003); J. Lin, Y.-K. Ko, L. Sui, J. C. Raymond, G. A. Stenborg, Y. Jiang, S. Zhao, and S. Mancuso, *Astrophys. J.* **622**, 1251 (2005); A. Ciaravella and J. C. Raymond, *Astrophys. J.* **686**, 1372 (2008); G. Schettino, G. Poletto, and M. Romoli, *Astrophys. J.* **708**, 1135 (2010); S. L. Savage, D. E. McKenzie, K. K. Reeves, T. G. Forbes, and D. W. Longcope, *Astrophys. J.* **722**, 329 (2010); K. K. Reeves and L. Golub, *Astrophys. J.* **727**, L52 (2011); E. Landi, J. C. Raymond, M. P. Miralles, and H. Hara, *Astrophys. J.* **751**, 21 (2012); S. L. Savage, G. Holman, K. K. Reeves, D. B. Seaton, D. E. McKenzie, and Y. Su, *Astrophys. J.* **754**, 13 (2012); A. Ciaravella, D. F. Webb, S. Giordano, and J. C. Raymond, *Astrophys. J.* **766**, 65 (2013).
- ⁶⁸P. Riley, R. Lionello, Z. Mikić, J. Linker, E. Clark, J. Lin, and Y.-K. Ko, *Astrophys. J.* **655**, 591 (2007); J. Lin, J. Li, T. G. Forbes, Y.-K. Ko, J. C. Raymond, and A. Vourlidis, *Astrophys. J.* **658**, L123 (2007).
- ⁶⁹McKenzie, David E., *Astrophys. J.* **766**, 39.
- ⁷⁰T. Yokoyama and K. Shibata, *PASJ* **48**, 353 (1996); K. Shibata, T. Nakamura, T. Matsumoto, K. Otsuji, T. J. Okamoto, N. Nishizuka, T. Kawate, H. Watanabe, S. Nagata, S. UeNo, R. Kitai, S. Nozawa, S. Tsuneta, Y. Suematsu, K. Ichimoto, T. Shimizu, Y. Katsukawa, T. D. Tarbell, T. E. Berger, B. W. Lites, R. A. Shine, and A. M. Title, *Science* **318**, 1591 (2007).
- ⁷¹H. Ji and W. Daughton, *Phys. Plasmas* **18**, 111207 (2011).
- ⁷²M. Yamada, *Space Sci. Rev.* **160**, 25 (2011).
- ⁷³V. S. Lukin and S. C. Jardin, *Phys. Plasmas* **10**, 3131 (2003).
- ⁷⁴S. Dorfman, W. Daughton, V. Roytershteyn, H. Ji, Y. Ren, and M. Yamada, *Phys. Plasmas* **15**, 102107 (2008).
- ⁷⁵V. S. Lukin, G. Qin, W. H. Matthaeus, and M. R. Brown, *Phys. Plasmas* **8**, 1600 (2001).
- ⁷⁶H. Hasegawa, *Monographs on Environment, Earth and Planets* **1**, 71 (2012).
- ⁷⁷M. Øieroset, T. D. Phan, M. Fujimoto, R. P. Lin, and R. P. Lepping, *Nature* **412**, 414 (2001).
- ⁷⁸F. S. Mozer, V. Angelopoulos, J. Bonnell, K. H. Glassmeier, and J. P. McFadden, *Geophys. Res. Lett.* **35**, 17 (2008).
- ⁷⁹T. P. Intrator, X. Sun, G. Lapenta, L. Dorf, and I. Furno, *Nature Physics* **5**, 521 (2009); X. Sun, T. P. Intrator, L. Dorf, J. Sears, I. Furno, and G. Lapenta, *Phys. Rev. Lett.* **105**, 255001 (2010).